29th Congress of the International Council
of the Aeronautical Sciences
St. Petersburg, Russia; September 7–12, 2014

LARGE EDDY SIMULATIONS OF TURBULENT FLOWS WITH ADVERSE PRESSURE GRADIENTS

Antonio B. Jesus* , Luiz A. C. A. Schiavo* , João L. F. Azevedo** , William R. Wolf***
*Instituto Tecnológico de Aeronáutica, São José dos Campos, SP, Brazil
**Instituto de Aeronáutica e Espaço, São José do Campos, SP, Brazil
***Universidade Estadual de Campinas, Campinas, SP, Brazil

Keywords: *LES, Turbulent flows, Adverse pressure gradients*

Abstract

The work presents comparative results between wall friction and pressure coefficient predictions from Large Eddy Simulation (LES) and Reynolds-averaged Navier-Stokes (RANS) computations in channel flows with an adverse pressure gradient created by a 2-D bump. Reynolds numbers range from $Re_\tau = 617$ to 2000, based on the friction velocity at the channel inlet. LES produces very consistent results when compared to DNS or other highly resolved LES. Two-equation and seven-equation RANS models are found to correctly predict friction coefficients in zero and favorable pressure gradient regions, but they fail in regions of adverse pressure gradients. The Reynolds stress transport model shows a better performance when compared to two-equation eddy-viscosity models, particularly in the higher Reynolds number cases. However, none of the RANS models is able to capture the full physics of turbulence related with adverse pressure gradients. Such limitations seem to be related to the fact that these models do not correctly describe the evolution of the turbulent kinetic energy close to the walls in adverse pressure gradient regions.

1 Introduction

The need for predicting aircraft drag and the performance of turbo-machinery and many other industrial components has been an important motivation for the development of RANS turbulence models in the last decades. Much effort was concentrated in the capability of predicting flow separation due to adverse pressure gradients and this is probably one of the reasons of the huge success found by the SST turbulence model in the aerospace industry [1].

Besides the prediction of separation and reattachment locations, it should also be considered that the correct calculation of the skin friction coefficient in attached flows is of paramount importance to the application of numerical simulations in industry. The fact that around 70% of the drag in a commercial airplane comes from friction gives a dimension of the criticality in the accurate calculation of skin friction coefficients in turbulent flows.

Recent work showed that understanding and modeling the complete physics of turbulence associated with adverse pressure gradient (APG) flows is still a challenge. The DNS calculation of the flow around a smooth bump, performed at Laboratoire de Mécanique de Lille (LML) [2, 3], may be considered as an important milestone in the understanding of the correlation between mean flow statistics and turbulent structures in adverse pressure gradient conditions. Particularly, the DNS results evidenced the presence of strong peaks of turbulent kinetic energy in regions of adverse pressure gradients which were linked to instability modes of the near wall streaks [3]. Subsequent studies showed that LES simulations are able to yield adequate mean flow variables, *e.g.*, friction and pressure coefficients, very similar to those obtained from DNS in similar flows, but using much coarser

computational meshes [4, 5]. In addition, it was found that LES correctly predicts the peaks of turbulent kinetic energy in APG regions found in the DNS calculations [4, 5].

In the domain of the Reynolds-averaged Navier-Stokes (RANS) formulation, it is found that, despite recent improvements, the turbulence models are still not capable of adequately predicting the flow characteristics in APG regions [5, 6]. Two-equation models tend to either under-predict or over-predict flow separation. Reynolds stress transport models show better results, especially in the pressure distribution. However, none of the RANS models proved to be fully accurate in skin friction calculations [5]. The inaccuracies of RANS models in APG regions have been associated with the inability of such models of correctly predicting flow separation and re-attachment locations [1, 6]. On the other hand, recent studies [5] suggest that the behavior of the skin friction coefficient in APG regions of smooth bumps does not depend on flow separation. In other words, the behavior in either attached or mildly separated flows is very similar, indicating that the prevailing physical mechanism is mostly associated with the adverse pressure gradient condition.

The present work aims at extending a previous study [5] by considering higher Reynolds numbers, finer LES meshes and a deeper analysis of results from RANS models. The same geometric configuration is used, but the Reynolds number is increased up to $Re_\tau = 2000$, based on the friction velocity at the channel inlet. This is a case of particular interest as there is no flow separation on the rear portion of the bump. In addition, previous LES calculations performed at $Re_\tau = 950$ are reworked using finer meshes. LES results are compared to corresponding RANS solutions using two-equation and seven equation models. Comparison is initially performed in terms of skin friction and pressure coefficient distributions, followed by a deeper analysis of the evolution of Reynolds stresses along the bump wall.

As in the previous study [5], LES calculations use the MFLOPS3D semi-spectral code, developed at LML. The Wall-Adapting Local Eddy-viscosity (WALE) closure [7] is used to model the sub-filter stresses. RANS computations are performed using the Ansys Fluent v.14.0 commercial code, with two different two-equation models, namely, the realizable k-ε and the SST models, and with the Reynolds stress transport model (RSM) available in Ansys Fluent [8].

2 Geometric and Physical Models

2.1 Bump Geometry

The bump profile under study is displayed in Fig. 1. It combines an initial favorable pressure gradient region in the upstream portion of the bump with an APG region in the back of it. This bump profile was studied both in wind-tunnel experiments, at high Reynolds numbers, and by DNS calculations [2, 3], at low Reynolds numbers, $Re_\tau = 395$ and 617, during the recent WALL-TURB European project [9]. For all calculations performed here, as well as in the DNS computations, the bump is considered as installed in a channel with 2.0 m in height and 4π m in length.
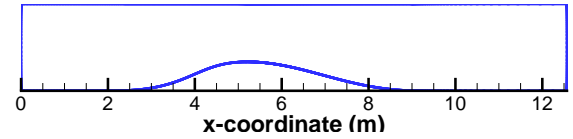

Fig. 1 Bump geometry.

2.2 LES Formulation

LES computations are performed using the MFLOPS3D code developed at LML. This is a semi-spectral code, developed for the study of 3-D boundary layer or channel flows around 2-D bumps. The code has been used for performing laminar flow instability computations [10], DNS of turbulent channel flows around 2-D bumps [2, 3], and LES of the same types of flows [4].

The code, when running in LES mode, solves the filtered incompressible Navier-Stokes equations, which can be written as

$$\frac{\partial \vec{\bar{u}}}{\partial t} + \left(\vec{\bar{u}} \cdot \nabla\right) \vec{\bar{u}} = -\nabla \bar{p} + \frac{1}{Re}\Delta\vec{\bar{u}} - \nabla \cdot \tau^{sfs} \quad (1)$$

$$\nabla \cdot \vec{\bar{u}} = 0 \quad (2)$$

2

which represent the momentum equations and mass conservation equation, respectively. The 3-D filtered velocity vector is identified here as

$$\vec{\bar{u}} = \left\{ \begin{array}{c} \bar{u} \\ \bar{v} \\ \bar{w} \end{array} \right\} , \qquad (3)$$

or as $\bar{u}_i$ in indicial notation. The sub-filter stresses are defined as

$$\tau_{ij}^{sfs} = \overline{u_i u_j} - \bar{u}_i \bar{u}_j . \qquad (4)$$

In the present work, sub-filter terms are evaluated using the WALE model [7], which is adequate for wall bounded flow computations as it was conceived to recover the correct eddy-viscosity near wall scaling without the need for an explicit damping. The MFLOPS3D code uses a variable transformation that maps the physical domain, shown in Fig. 1, into a Cartesian domain.

The Navier-Stokes equations are discretized using an 8th-order centered finite difference scheme in the streamwise direction for the first derivatives. The viscous terms are discretized using a 4th-order centered finite difference scheme. Chebyshev polynomials, collocated in Chebyshev-Lobatto points [11], are used in the normal direction. A Fourier transform is performed in the spanwise direction, which is assumed to be periodic, using the 3/2 rule to remove aliasing error of the discrete Fourier transform [11].

Time integration is performed using an implicit 2nd-order backward Euler method for the terms containing the Cartesian components of the Laplacian operator, while an explicit 2nd-order Adams-Bashforth method is used for all other terms, including the sub-filter stresses. Pressure-velocity coupling is achieved by a fractional-step method which performs an iterative process. In this process, the solution of the momentum equations yields an intermediate velocity field, whereas the solution of the pressure Poisson equation determines an intermediate pressure [12]. Afterwards, iterations based on the continuity equation are used in order to obtain a pressure correction that produces a divergence-free velocity field. Computations are performed in Fourier space, and each Fourier mode is solved independently using parallel computations. The nonlinear and sub-filter terms are computed in physical space. The computational process is parallelized by mesh partition and the Message Passing Interface (MPI) protocol is used to communicate between processors.

Further details of the transformed equations and numerical methodology can be found in previous work which uses the MFLOPS3D code [2]. Boundary conditions for the inlet flow are obtained from a precursory periodic channel flow computation. No-slip conditions are imposed at the top and bottom walls, and the spanwise direction is assumed periodic with a π m width. The outflow boundary of the computational domain is treated as a convective boundary with uniform velocity, *i.e.*, the velocity vector is assumed to be transported by a constant convective velocity, U_c, as

$$\frac{\partial \vec{\bar{u}}}{\partial t} + U_c \frac{\partial \vec{\bar{u}}}{\partial x} = 0 . \qquad (5)$$

2.3 RANS Formulation

RANS calculations are performed using the Ansys Fluent v.14.0 commercial CFD package. Two 2-equation turbulence models, namely, realizable k-ε [13] and SST [1] models, are evaluated along with one of the Reynolds stress transport models (RSM) available in the code [14]. The steady-state, 2-D, incompressible, pressure-based, SIMPLE solver is used with the default settings of the Fluent package.

At the walls, the realizable k-ε and the RSM calculations use the so-called enhanced wall treatment option, which employs a two-layer formulation for the near wall region. Hence, in this region, the length scales used to compute the turbulent viscosity and the turbulent dissipation (ε) are adjusted to take into account the effects of the wall proximity [8]. In addition, the RSM model specifies values for the Reynolds stresses in the first cell off the wall, through the use of the log-law and the assumption of equilibrium [8].

Similarly to the LES computations, a precursory periodic channel flow is run to generate inlet conditions that are used for the calculations with the bump in the channel. No-slip conditions are

imposed at the walls and a constant pressure is assumed at the outlet. A 2-D mesh with 400×100 quadrilaterals in the streamwise and wall-normal directions, respectively, is used for the RANS calculations over the bump under study. Figure 2 shows the mesh used for RANS computations. The centroid of the first off-the-wall cell is placed at 0.25 mm from the wall, which approximately corresponds to a maximum $y^+ = 0.3$ for the present calculations.
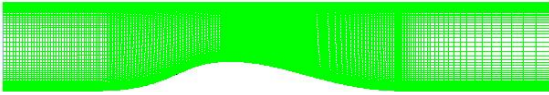

Fig. 2 Overall view of the RANS mesh.

3 Results

LES computations at $Re_\tau = 617$, 950 and 2000 are performed. Periodic channel flows, at the same Reynolds numbers, are computed and, after statistical convergence, the velocity vectors at a plane normal to the streamwise direction are stored for the equivalent of two flow-through times, for each case. Such velocity history is imposed as entrance condition at the inlet for the bump calculations. Computations at $Re_\tau = 617$ use 320×129 nodes in the streamwise and normal directions, respectively, and 128 Fourier modes in the spanwise direction. Simulations at $Re_\tau = 950$ use two refinement levels. The first one corresponds to a coarse mesh and it uses 448×97 grid points in the streamwise and normal directions, and 128 modes in the spanwise direction. A finer level employs 1024×193 grid points in the streamwise and normal directions, and 256 modes in the spanwise direction. Computations at $Re_\tau = 2000$ used the same refinement from the fine mesh of the $Re_\tau = 950$ simulations. A time step of 0.001 s is used in all test cases.

For the computations at $Re_\tau = 2000$ and at $Re_\tau = 950$ with the finer mesh, it was necessary to add a stretching zone (SZ) in the channel outlet. The purpose of this region is to dissipate turbulent structures before reaching the boundary of the domain, as short wavelength structures can be reflected at the exit boundary causing numerical instabilities. Therefore, for those cases, the computational domain is longer than the domain used to compute flow statistics, which is the same in all calculations. Table 1 presents mesh sizes in the domain for statistics computations, the length and the number of points in the stretching zone, when it is present, and the refinement levels in terms of wall units at the top of the bump.

Kuban *et al.* [4] performed LES with different mesh refinement for the same bump configuration at $Re_\tau = 617$. Such work showed that, with the use of Δx^+, Δy^+ and Δz^+ values around 45, 0.25 and 30, respectively, at the top of the bump, it was possible to compute statistics in good agreement with DNS results for the same configuration. Table 1 shows that the mesh refinement levels used in the present work are similar to those from Kuban *et al.*[4]. In addition, current LES results are compared to DNS or other LES with more resolution, when available. Therefore, it is believed that current LES meshes are adequate to compute flow statistics in the range of Reynolds number analyzed. Figure 3 presents the LES-calculated skin friction coefficient distributions at the bottom wall for the Reynolds numbers under study. Similarly, Fig. 4 brings the corresponding pressure coefficient distributions at the same Reynolds numbers.
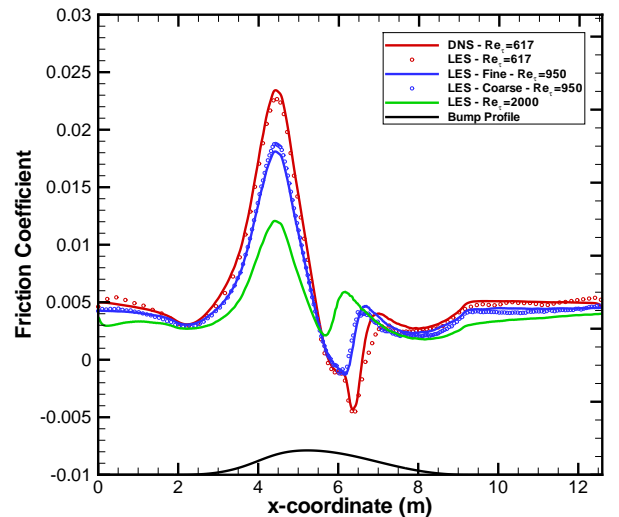

Fig. 3 Bottom wall friction coefficient distributions. LES: $Re_\tau = 617$, 950 and 2000; DNS: $Re_\tau = 617$.

4

Table 1 Mesh configuration for LES cases.

Re_τ	Nx	Ny	Nz	Statistics Domain (m)	SZ length (m)	Nx (SZ)	Δx^+	Δz^+	Δy^+
617	320	129	128	$4\pi \times 2 \times \pi$	–	–	23.0	21.2	0.17
950	448	97	128	$4\pi \times 2 \times \pi$	–	–	24.0	31.0	0.45
950	964	193	256	$4\pi \times 2 \times \pi$	4π	60	16.3	15.0	0.11
2000	956	193	256	$4\pi \times 2 \times \pi$	2π	68	30.4	30.7	0.22
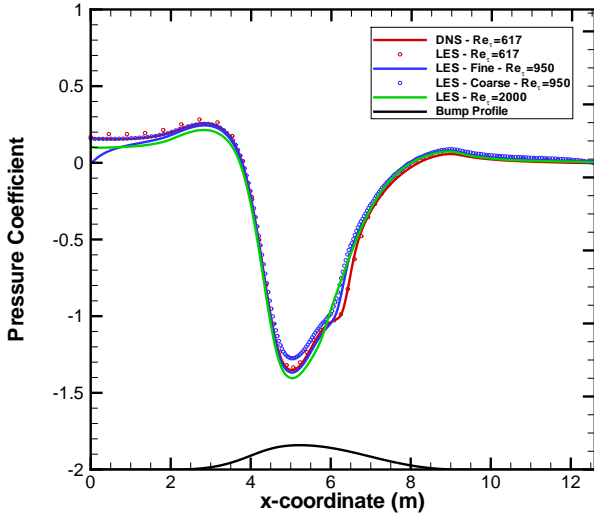
Fig. 4 Bottom wall pressure coefficient distributions. LES: $Re_\tau = 617$, 950 and 2000; DNS: $Re_\tau = 617$.
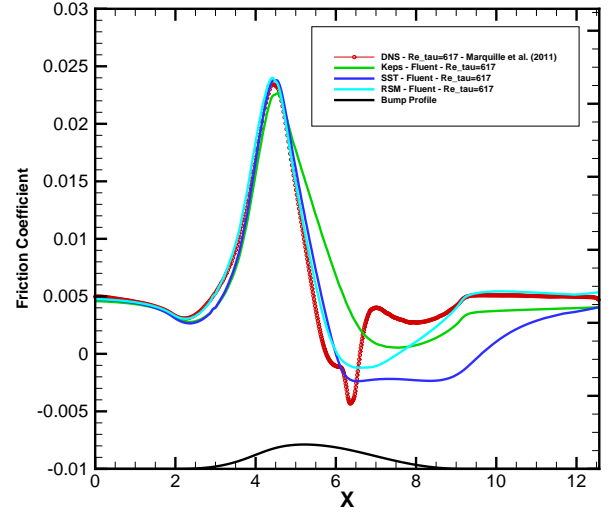
Fig. 5 Bottom wall friction coefficient distributions. RANS: $Re_\tau = 617$; DNS: $Re_\tau = 617$.

In order to assess the behavior of the RANS models, Fig. 5 compares the friction coefficient distributions along the bottom wall, obtained from RANS computations and DNS at $Re_\tau = 617$. It can be seen that, in the favorable pressure gradient region, the RANS results have very good agreement with the DNS data. However, this behavior does not hold for the adverse pressure gradient region. The realizable k-ε model captures the drop in friction coefficient due to the adverse pressure gradient, but it does not show flow separation. Moreover, downstream of the bump, the friction coefficient slowly recovers towards a constant value. The SST results compare very well with DNS up to the separation point. This is an expected result as this model is widely known to predict flow separation better than k-ε models [1]. Downstream of the separation point, however, a much larger separation bubble is pre-

dicted by the SST calculations than what is seen in DNS. Flow re-attachment only occurs downstream of the bump, with the slow recovery of the friction coefficient.

The RSM model has a performance similar to that of the SST model up to the separation point. After separation, the recovery of the skin friction coefficient is slower than the one present in the DNS results, with a larger separation bubble. However, when compared to the two-equation model results, it can be seen that the RSM model yields a better comparison with DNS. It is clear from these results that, when compared to the LES calculations, none of the RANS models correctly predicts either the negative peak of the skin friction in the separated flow region or its recovery after reattachment. In terms of pressure coefficients, Fig. 6 shows that RANS models do not correctly predict the inflection observed in DNS results for the pressure coefficient distribution in the separated flow region.
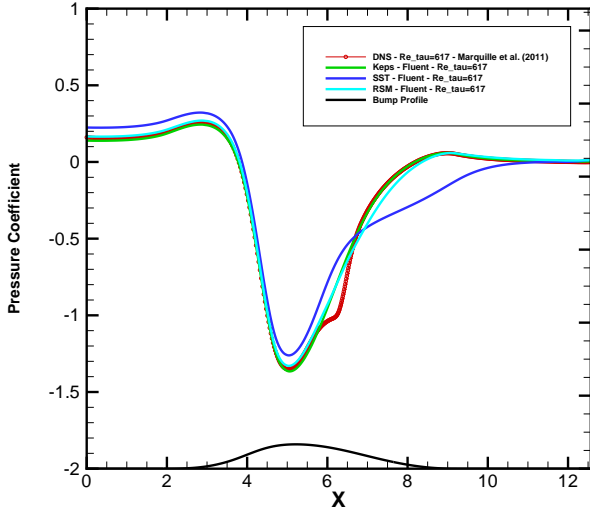
Fig. 6 Bottom wall pressure coefficient distributions. RANS: $Re_\tau = 617$; DNS: $Re_\tau = 617$.

Figure 7 shows Reynolds stress profiles along lines normal to the bump wall from RANS computations with the RSM model compared to DNS results. Reynolds stresses are calculated using tangential, normal and transversal velocity fluctuation components. The stresses are normalized with respect to the friction velocity at the inlet of the channel. Moreover, the distance to the wall is also normalized with regard to the friction velocity at the inlet of the channel. In these figures, the first plot corresponds to the $x = 4.4$ m station, which is the location of the first peak in C_f as identified from Fig. 3 for all the Reynolds numbers under study. The subsequent plots show the evolution of Reynolds stresses along the adverse pressure gradient region up to the $x = 9.4$ m station, which is located downstream of the bump.

Figure 7 compares the evolution of Reynolds stresses near the bump wall obtained from DNS results and the RSM model at $Re_\tau = 617$. It is observed that both results show the initial peak of the Reynolds stresses moving away from the wall and increasing in intensity up to station $x = 6.2$ m. It can be observed that Reynolds stress levels predicted by the RSM calculations are somewhat higher than those obtained from DNS. This seems to correlate with the fact that the negative peak in C_f obtained from the RSM calculations, shown in Fig. 5, does not drop to the same level as observed in the DNS results. The scenario

changes abruptly at the $x = 6.4$ and $x = 7.0$ m stations, where the sharp increase in turbulence intensity observed in the DNS results is not reproduced by the RSM solution. Again, this can be correlated to the C_f profiles from Fig. 5, as the sharp increase in C_f from DNS calculations is not seen in the RSM results. The latter presents a longer separated flow region. At the rear portion of the bump, the Reynolds stress levels from both DNS and RSM solutions tend to similar values and this is also reflected in similar behavior of the friction coefficients in this region.

Figures 8 and 9 present skin friction and pressure coefficient distributions, respectively, along the bottom wall for the RANS and LES calculations at $Re_\tau = 950$. Similar trends as those observed in the $Re_\tau = 617$ calculations can be noticed in the present case. All RANS models produce results very similar to LES in the favorable pressure gradient region. In the APG region, the realizable k-ε model does not predict either the decrease or the rise in skin friction values observed in LES results. The SST model predicts a large flow separation region, missing slightly the separation point position. The RSM calculations present the best results in terms of skin friction distribution, despite the fact that such results do not predict any flow separation or the sharp rise in C_f in the flow re-attachment region. None of the RANS models captures all the details of the pressure coefficient distribution, but the predictions from k-ε and RSM closures appear to be in better agreement with LES results than the SST calculations.

Figures 10 and 11 present the corresponding skin friction and pressure coefficient distributions from RANS and LES solutions at $Re_\tau = 2000$. At this Reynolds number, flow separation in the downstream portion of the bump does not occur. Nevertheless, rapid decrease and recovery of skin friction coefficient in the APG region is still observed, similar to the behavior present in lower Reynolds number flows. RANS models continue to produce results very similar to LES in the zero or favorable pressure gradient regions. In the APG region, the realizable k-ε model does not reproduce either the slope or the levels of skin friction observed in LES results. The SST model
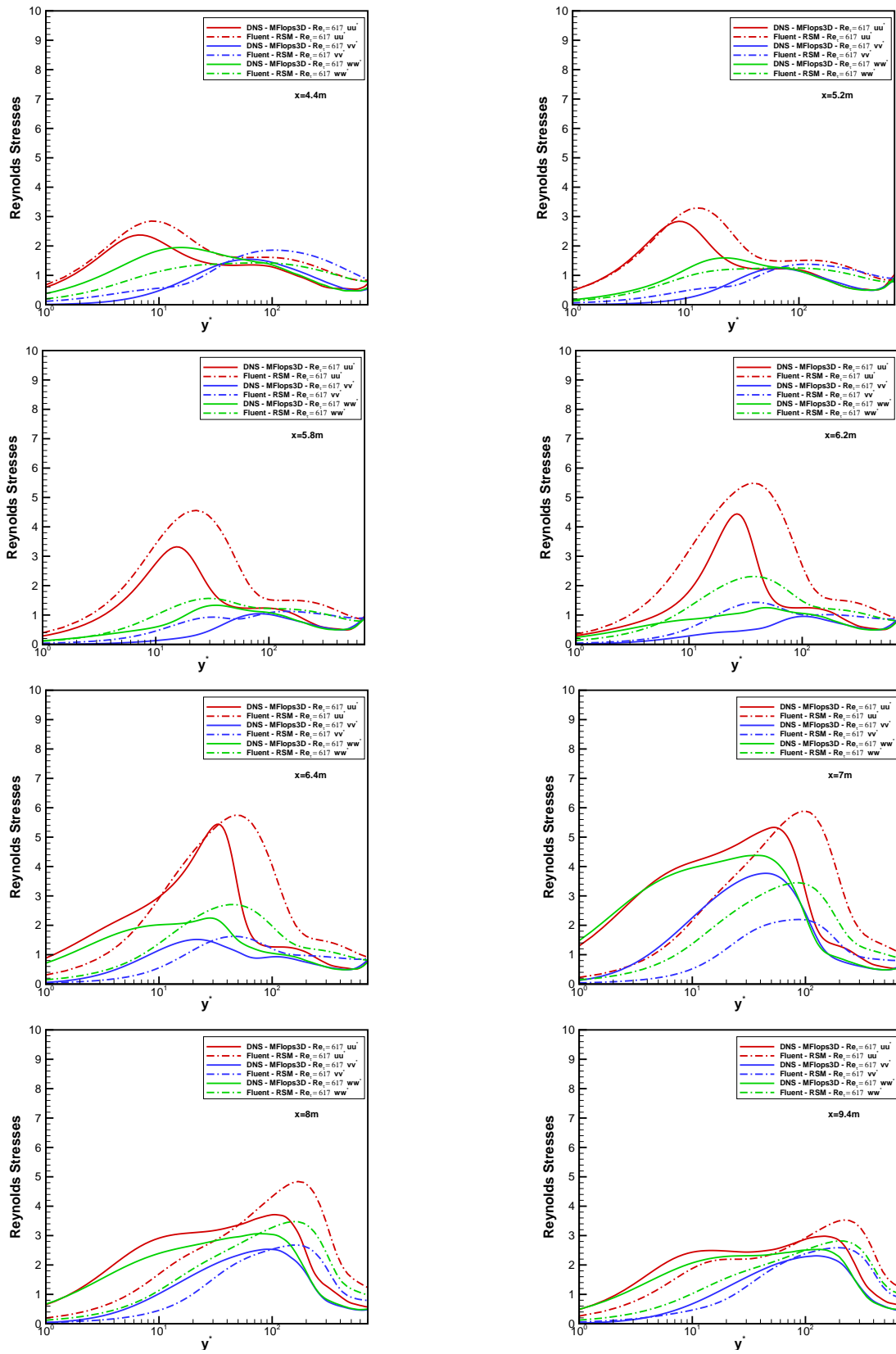
Fig. 7 Bump profile - Reynolds Stresses - Re$_\tau$= 617 - RANS: Fluent - DNS [3]

Fig. 8 Bottom wall friction coefficient distributions. RANS: $Re_\tau = 950$; LES: $Re_\tau = 950$.
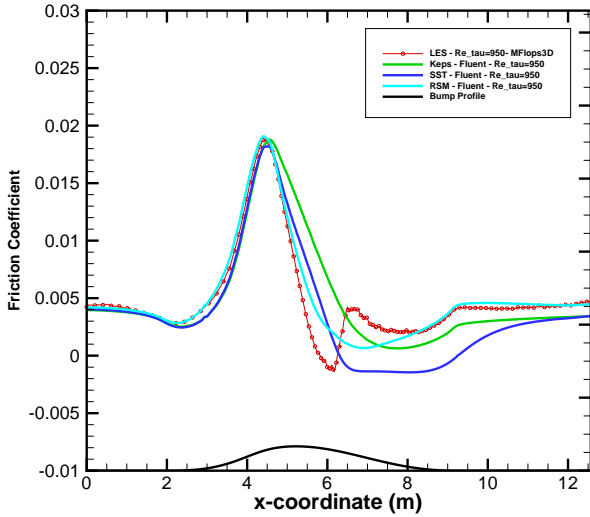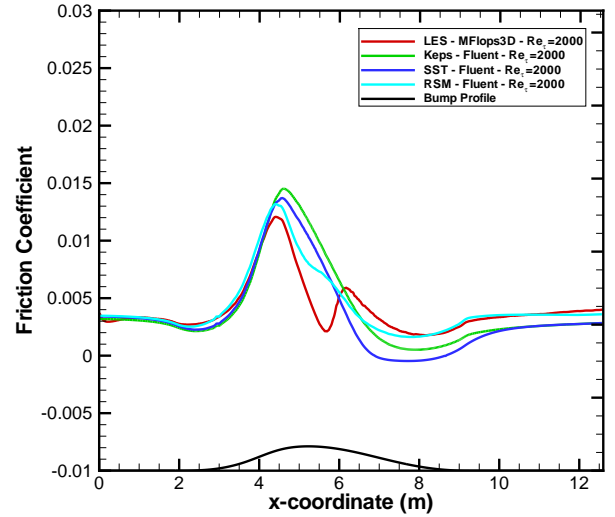

Fig. 9 Bottom wall pressure coefficient distributions. RANS: $Re_\tau = 950$; LES: $Re_\tau = 950$.

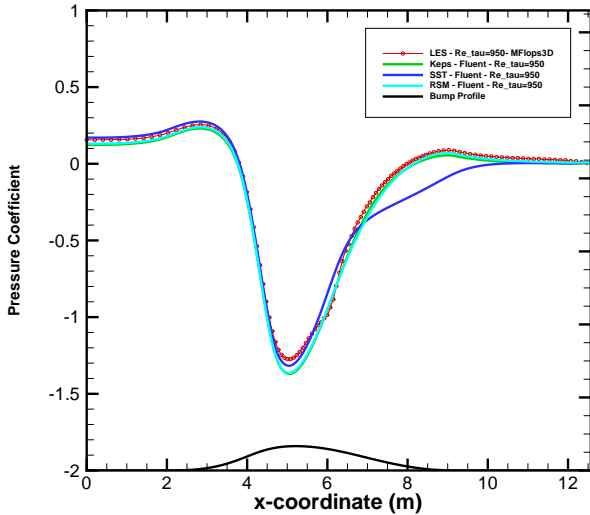**Fig. 10** Bottom wall friction coefficient distributions for RANS and LES calculations at $Re_\tau = 2000$.

Fig. 11 Bottom wall pressure coefficient distributions for RANS and LES calculations at $Re_\tau = 2000$.

also misses the skin friction rapid decrease and it still predicts some flow separation at the rear of the bump. The RSM calculations present the best results in terms of skin friction coefficient distribution, with a better relative performance than observed for the lower Reynolds number test cases. The initial decrease of C_f in the APG region is well capture and, despite not predicting the full drop of the friction coefficient, the change in slope in the distribution at the rear portion of the bump and its recovery are well predicted. The superiority of RSM results relati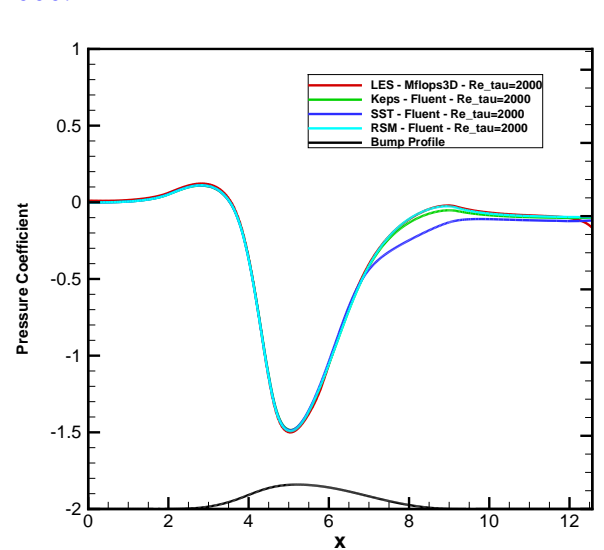ve to those obtained with two-equation models can also be observed in Fig.11, in terms of pressure coefficient distributions.

Additional studies for the same configuration, using both DNS and LES computations and presented in Ref. [15], showed a clear correlation between the behavior of the skin friction coefficient and the evolution of the Reynolds stresses close to the bump wall in the adverse pressure gradient region. Therefore, the fact that RANS models do not reproduce the same C_f distributions from DNS or LES calculations should also be related

to differences in the Reynolds stress evolution computed from RANS models when compared to DNS or LES. Here, only the Reynolds stress results for $Re_\tau = 617$ have been presented for the sake of brevity, but similar behavior is observed for the other Reynolds numbers addressed in the present investigation.

Recent DNS results [3] have shown strong peaks of turbulent kinetic energy associated with adverse pressure gradients and other studies [4] have indicated that those peaks are also present in LES calculations. Results from the current work corroborate the conclusions from these previous DNS and LES studies as it is observed that a similar pattern for the evolution of the near wall turbulent kinetic energy in the adverse pressure gradient region persists for higher Reynolds numbers. In addition, a clear correlation is identified between the skin friction behavior and the near wall turbulence intensity levels in the APG region. In terms of RANS modeling, as previously discussed, the literature tends to correlate the inaccuracies of RANS computations in APG regions to the inability of correctly predicting flow separation and re-attachment locations, and the physics of turbulence associated to separation phenomena [6]. Current results show that RANS models do not correctly predict either the skin friction coefficient or the evolution of turbulent kinetic energy near the wall. Such shortcomings are observed in attached and mildly-separated flows. This reinforces the conclusion that RANS models may also lack some of the physics present in APG regions, particularly those pertaining to turbulent kinetic energy production.

4 Concluding Remarks

The paper presented LES results for the skin friction coefficient along the bottom wall of a two-dimensional bump in a channel. Calculations performed at $Re_\tau = 617$ show a good comparison with DNS computations. At the rear portion of the bump, C_f distributions present similar patterns in higher Reynolds numbers, $Re_\tau = 950$ and 2000, even when there is no flow separation. Particularly, a sharp decrease and recovery of C_f is observed in the APG regions at all Reynolds numbers.

Two-equation and seven-equation RANS models are also studied and compared with the LES solutions. RANS-calculated skin friction coefficients almost perfectly matched DNS or LES results in zero or favorable pressure gradient regions. In regions of adverse pressure gradients, however, it is found that none of the RANS models considered is able to reproduce the behavior observed in LES or DNS calculations. The seven-equation RSM model studied has a better performance when compared to standard two-equation eddy-viscosity models, particularly in the higher Reynolds number range here analyzed. However, the RANS models are not really able to capture the full physics of turbulence related with adverse pressure gradient regions.

The results obtained at $Re_\tau = 2000$ indicate that the inability of RANS models in describing skin-friction coefficient distributions in APG regions is not only related to prediction of flow separation and re-attachment. Since this test case actually does not have flow separation, and the RANS results follow the general trends observed at lower Reynolds numbers, there seems to be enough evidence that the prevailing physical mechanism is associated with the existence of an adverse pressure gradient region. The observed behavior seems to be related to the fact that the RANS models do not correctly describe the production and evolution of the turbulent kinetic energy close to the walls in adverse pressure gradient regions.

Acknowledgments

Nacional de Supercomputação, CESUP, of Universidade Federal do Rio Grande do Sul, in Porto Alegre, are also gratefully acknowledged.

References

[1] Menter, F. R., Kuntz, M., and Langtry, R., "Ten Years of Industrial Experience with the SST Turbulence Model," *Turbulence, Heat and Mass Transfer 4*, Begell House, Inc., 2003.

[2] Marquillie, M., Laval, J. P., and Dolganov, R., "Direct Numerical Simulation of Separated Channel Flows with a Smooth Profile," *Journal of Turbulence*, Vol. 9, No. 1, 2008, pp. 1–23.

[3] Marquillie, M., Ehrenstein, U., and Laval, J. P., "Instability of Streaks in Wall Turbulence with Adverse Pressure Gradient," *Journal of Fluid Mechanics*, Vol. 681, Aug. 2011, pp. 205–240.

[4] Kuban, L., Laval, J. P., Elsner, W., Tyliszcak, A., and Marquillie, M., "LES Modeling of Converging-Diverging Turbulent Channel Flow," *Journal of Turbulence*, Vol. 16, No. N11, 2012, pp. 1–19.

[5] Jesus, A. B., Azevedo, J. L. F., and Laval, J. P., "Large Eddy Simulations and RANS Computations of Adverse Pressure Gradient Flows," AIAA Paper No. AIAA 2013-0267, *51st AIAA Aerospace Sciences Meeting including the New Horizons Forum and Aerospace Exposition*, Grapevine, TX, Jan. 2013.

[6] Jeyapaul, E. and Rumsey, C., "Analysis of Highly-Resolved Simulations of 2-D Humps Toward Improvement of Second-Moment Closures," AIAA Paper No. AIAA 2013-0684, *51st AIAA Aerospace Sciences Meeting including the New Horizons Forum and Aerospace Exposition*, Grapevine, TX, Jan. 2013.

[7] Nicoud, F. and Ducros, F., "Subgrid-Scale Stress Modelling Based on the Square of the Velocity Gradient Tensor," *Flow, Turbulence and Combustion*, Vol. 62, 1999, pp. 183–200.

[8] ANSYS, Inc., *ANSYS FLUENT Theory Guide Release 14.0*, November 2011.

[9] Stanislas, M., Jimenez, J., and Marusic, I., editors, *Progress in Wall Turbulence: Understanding and Modeling*, ERCOFTAC. Springer, 2009.

[10] Marquillie, M. and Ehrenstein, U., "On the Onset of Nonlinear Oscillations in a Separating Boundary-Layer Flow," *Journal of Fluid Mechanics*, Vol. 490, 2003, pp. 169–188.

[11] Canuto, C., Hussaini, M. Y., Quarteroni, A., and Zang, T. A., *Spectral Methods in Fluid Dynamics*, Springer-Verlarg, Berlin Heidelberg, 4th ed., 1988.

[12] Karniadakis, G. E., Israeli, M., and Orszag, S. A., "High-Order Splitting Methods for the Incompressible Navier-Stokes Equations," *Journal of Computational Physics*, Vol. 97, 1991, pp. 414–443.

[13] Shih, T. H., Liou, W. W., Shabbir, A., Yang, Z., and Zhu., J., "A New $k - \varepsilon$ Eddy-Viscosity Model for High Reynolds Number Turbulent Flows - Model Development and Validation," *Computers and Fluids*, Vol. 24, No. 3, 1995, pp. 227–238.

[14] Launder, B. E. and Shima, N., "Second-Moment Closure for the Near-Wall Sublayer: Development and Application," *AIAA Journal*, Vol. 27, No. 10, 1989, pp. 1319–1325.

[15] Jesus, A. B., Schiavo, L. A. C. A., Azevedo, J. L. F., and Laval, J. P., "An Assessment of Attached and Mildly Separated Flows in Adverse Pressure Gradient Regions," AIAA Paper No. AIAA 2014-0583, *52nd AIAA Aerospace Sciences Meeting*, National Harbor, MD, Jan. 2014.

5 Contact Author Email Address

A. B. Jesus, antoniobjota@gmail.com
L. A. C. A. Schiavo, augustoschiavo@gmail.com
J. L. F. Azevedo, joaoluiz.azevedo@gmail.com
W. R. Wolf, wolf@fem.unicamp.br

Copyright Statement